

Contents list available at CBIORE journal website

International Journal of Renewable Energy Development

Journal homepage: https://ijred.cbiore.id



Research Article

Assessment of photovoltaic efficacy in antimony-based cesium halide perovskite utilizing transition metal chalcogenide

Abdullah Alghafis^a o and K. Sobayel^{b*}

- ^a Department of Mechanical Engineering, College of Engineering, Qassim University, Buraydah 51431, Saudi Arabia
- ^b Solar Energy Research Institute (SERI), The National University of Malaysia (UKM), Malaysia.

Abstract. Antimony-based perovskites have been recognized for their distinctive optoelectronic attributes, standard fabrication methodologies, reduced toxicity, and enhanced stability. The objective of this study is to systematically investigate and enhance the performance of all-inorganic solar cell architectures by integrating $Cs_3Sb_2I_9$, a perovskite-analogous material, with WS₂—a promising transition metal dichalcogenide—used as the electron transport layer (ETL), and Cu2O serving as the hole transport layer (HTL). This comprehensive assessment extends beyond the mere characterization of material attributes such as layer thickness, doping levels, and defect densities, to include a thorough investigation of interfacial defect effects within the structure. Optimal efficiency was observed when the $Cs_3Sb_2I_9$ absorber layer thickness was maintained within the 600-700 nm range. The defect tolerance for the absorber layer was identified at 1×10^{15} /cm³, with the ETL and HTL layers exhibiting significant defect tolerance at 1×10^{16} /cm³ and 1×10^{17} /cm³, respectively. Furthermore, this study calculated the minority carrier lifetime and diffusion length, establishing a strong correlation with defect density; a minority carrier lifetime of approximately 1 μ s was noted for a defect density of 1×10^{14} /cm³ in the absorber layer. A noteworthy finding pertains to the balance between the high work function of the back contact and the incorporation of p-type back surface field layers, revealing that interposing a highly doped p+ layer between the Cu₂O and the metal back contact can elevate the efficiency to 21.60%. This approach also provides the freedom to select metals with lower work functions, offering a cost-effective advantage for commercial-scale applications.

Keywords: Perovskite Solar Cell, Cesium antimonide halides, Transition metal, Chalcogenides, ETL, Efficiency, Stability



@ The author(s). Published by CBIORE. This is an open access article under the CC BY-SA license (http://creativecommons.org/licenses/by-sa/4.0/).

 $Received: 29^{th}\ April\ 2024; Revised: 7^{th}\ June\ 2024; Accepted: 15^{th}\ June\ 2024; Available\ online: 28^{th}\ June$

1. Introduction

The historical development of solar cell technology can be segmented into three distinct generations. The inaugural generation, epitomized by silicon-based cells, is characterized by high efficiency but is also marked by considerable expense and complexity in production. The second generation, thin-film cells like GaAs and CdTe, boasts affordability but faces issues with material scarcity and potential toxicity. The third generation, comprising various thin-film and multi-layer designs, shines with low-cost materials, ease of production, and promising efficiency. Among them, perovskite solar cells stand out as the most exciting potential future for the field(Thomas, 2022b). Perovskite solar cells grab researchers' interest due to their exceptional light-absorbing traits, adjustable energy levels, simple fabrication, readily available materials, and impressive results in terms of both cost and efficiency. These exciting devices often use methylammonium lead iodide (MAPbI3) as their active ingredient, offering a glimpse into the future of affordable and effective solar energy(Hayat et al., 2019). Despite promising efficiency and ease of production, lead-based perovskite solar cells face major hurdles before hitting the market. While they boast impressive light absorption, bandgaps, and processing traits, their instability under UV, heat, and

moisture, coupled with lead's toxicity, necessitate safer and more durable alternatives for wider adoption (Jin et al., 2020).

Life-cycle assessments paint a worrying picture for leadbased perovskite solar cells. From the procurement of raw materials to the fabrication of devices, the process engenders considerable lead contamination, detrimentally impacting the environment and presenting health hazards. Air, water, ecosystems, and even workers' health suffer, highlighting the need for eco-friendly alternatives with similar efficiency but without the toxic dangers. This pushes researchers towards developing "greener" perovskite technologies that safeguard both the planet and people (Leccisi & Fthenakis, 2020). Finding a safe replacement for lead in perovskite solar cells isn't as simple as swapping elements. While alternatives like Bi and Sb hold promise due to their similar characteristics and lower toxicity, others like Sn and Ge pose environmental and processing challenges. Researchers and policymakers need a comprehensive framework to analyze replacements, considering not just toxicity but also processing costs, material availability, and overall environmental impact. Only through careful evaluation can we unlock the true potential of perovskite technology without compromising sustainability(Schileo & Grancini, 2021).

* Corresponding author(s):

Email: sobayel@ukm.edu.my (K. Sobayel)

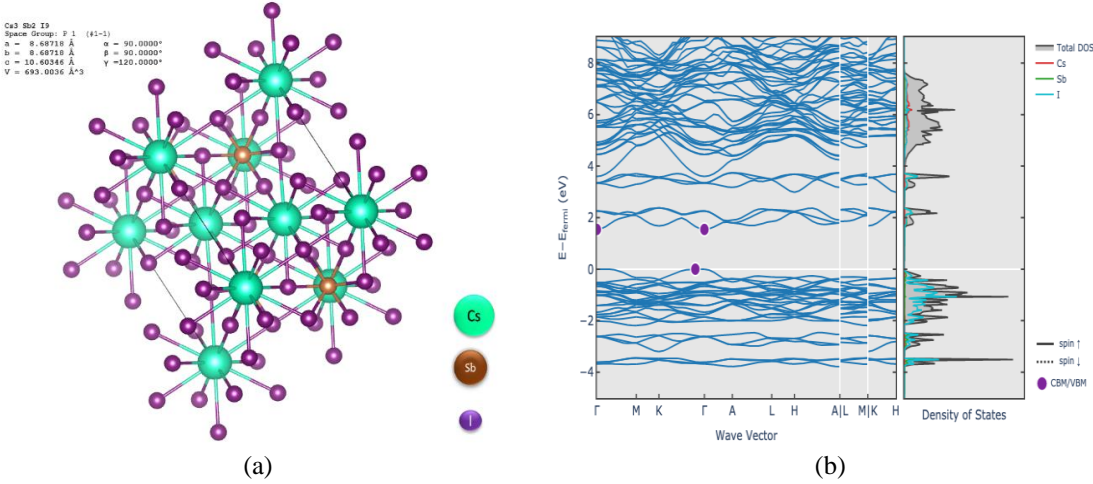


Fig 1 (a) Crystal structure and (b) E-K diagram of Cs₃Sb₂I₉

Antimony (Sb)-based halide perovskites have been developed historically and are presently employed on a provisional basis. These materials have been recognized as viable substitutes for light-absorbing layers in photovoltaic cells. Examples such as MA3Sb2I9 and Cs3Sb2I9 represent some of the conventional Sb-based light absorbers that have been engineered. Nonetheless, these substances exhibit exceedingly large bandgaps, elevated binding energies, and substantial carrier effective masses, all of which constrict their photovoltaic efficiency (Jin et al., 2020). This elucidates the limited adoption of VA-based halide perovskites, which exhibit performances significantly inferior to those of lead (Pb)-based perovskites.

Antimony (Sb), characterized by its trivalent nature, contains three electrons in its outermost electron shell, rendering it trivalent in chemical compounds. This electronic configuration facilitates the substitution of divalent lead (Pb2+) in perovskite structures. When antimony replaces lead, it forms an ionic complex with six halide ions (X), resulting in the formation of SbX63-. This complex assumes an octahedral geometry, where the antimony cation is centrally located, symmetrically surrounded by six halide anions at the vertices of an octahedron, thereby altering the electronic and structural properties of the material.

In this structural arrangement, halide ions are coordinated with the A-site cation, yielding a perovskite compound that exhibits diverse dimensionality and structural configurations. The molecular composition represented as A3B2X9 often leads to the formation of perovskite entities that manifest in either zero-dimensional (0D) or two-dimensional (2D) forms, delineating the variable spatial arrangement and connectivity of the constituent ions within the perovskite matrix (Jin et al., 2020). When integrated into a PSC (perovskite solar cell), Sbbased perovskites exhibit distinctive optoelectronic properties. Computational and experimental tests have been conducted to explore the optical characteristics of both 0D and 2D forms. The 0D form appears as a dimeric structure, while the 2D form represents a layered arrangement, such as Cs3Sb2I9. A hypothetical scenario suggests that CsSbI3 can be produced by modifying the structure of Cs3Sb2I9 layers. The twodimensional Cs3Sb2I9 variant possesses an optical bandgap of 2.05 eV and is recognized for its enhanced stability under ambient environmental conditions relative to MAPbI3. Research conducted by Boopathi et al. revealed that Cs3Sb2I9 exhibits a bandgap of 1.95 eV, while MA3Sb2I9 demonstrates a

bandgap of 2.0 eV. (Boopathi *et al.*, 2017) Buonassisi *et al.* determined that the optical bandgaps of cesium (Cs), rubidium (Rb), and potassium (K) based antimony iodide perovskites are 2.43, 2.03, and 2.02 eV, respectively, utilizing ultraviolet-visible (UV-Vis) absorption spectroscopy (Correa-Baena *et al.*, 2019).

Perovskite solar cells (PSCs) are characterized by their layered architecture, central to which is the perovskite absorber layer, imperative for the capture of solar radiation and the ensuing generation of charge carriers, such as electrons and holes. Encapsulating this core layer are the pivotal electron and hole transport layers (ETL and HTL), instrumental in the proficient migration and delineation of these charge carriers. The efficacy of electron extraction and conveyance from the perovskite domain is substantially governed by the electron transport materials (ETMs)' physicochemical characteristics (Islam *et al.*, 2021; Sobayel *et al.*, 2019; Zhao & Zhu, 2016). The deployment of high-efficiency electron transport materials (ETMs) is crucial for augmenting charge carrier mobility, diminishing recombination losses, and thereby, elevating the device's overall performance metrics.

In the architectural paradigm of PSCs, a planar structure is commonly implemented, where a thin perovskite film is encapsulated between layers of WS2 and Cu2O, serving as the ETL and HTL, respectively. This arrangement highlights the essential function of the electron transport layer (ETL) in managing the accumulation and conveyance of electrons toward the electrodes, a mechanism fundamental to the cell's operational efficiency. The performance metrics of PSCs, therefore, are intricately linked to the functional capabilities of the electron transport layers, necessitating a focused investigation into their material and electronic properties to drive advancements in PSC technology.

Recent progress in perovskite solar cell (PSC) technology has emphasized the importance of integrating innovative materials, especially in the electron transport layer (ETL), to improve the power conversion efficiency (PCE) of such devices (Correa-Baena et al., 2019; Dasgupta et al., 2017; Eperon et al., 2014; Huang et al., 2017; Leijtens et al., 2013; J. Liu et al., 2013; M. Liu et al., 2013) Among the materials explored, titanium dioxide (TiO2) has garnered significant attention as a prevalent inorganic ETL component in PSCs (Yang et al., 2016). The employment of this material aids in the movement of photogenerated electrons from the perovskite absorber layer to the ETL, demonstrating reduced interfacial recombination and

exhibiting comparatively suboptimal charge extraction characteristics. Despite these benefits, TiO2 is characterized by its moderate electron mobility and a propensity for rapid degradation under ultraviolet radiation exposure. (Geng *et al.*, 2016; Leijtens *et al.*, 2013; C. Liu *et al.*, 2015) Additionally, the integration of TiO2 often necessitates high-temperature annealing processes, typically close to 500°C, which not only prolongs the energy pay-back period but also poses constraints on the manufacturability of thin-film solar cells.

Despite the prevalent use of TiO2 and ZnO-based materials (Eperon et al., 2014; D. Liu & Kelly, 2013; M. Liu et al., 2013) in fabricating the utmost effective perovskite solar cells (PSCs) to date, alternative metal oxides like In2O3, SnO2, SrTiO3 have demonstrated their acceptancy as photoelectrodes in dyesensitized solar cells (DSSCs). However, these materials exhibit suboptimal performance metrics relative to TiO2 within the DSSC framework, highlighting the necessity for material innovation and optimization in PSC technology. Within this framework, transition metal dichalcogenides (TMDCs), such as molybdenum disulfide (MoS2) and tungsten disulfide (WS2), have attracted significant attention in the photovoltaic research domain.(Dasgupta et al., 2017; Huang et al., 2017). Their distinct electrical, optical, and electrochemical properties render them advantageous for application in visible light optical devices, suggesting a promising avenue for the enhancement of PSC performance through material engineering and the exploration of novel semiconductor interfaces. Within the gamut of transition metal dichalcogenides (TMDCs), tungsten disulfide (WS2) is distinguished by its superior carrier mobility, notable conductivity, approximately 10-3Ω-1cm-1 and inherent n-type semiconducting properties (Hankare et al., 2009; Sobayel et al., 2018). Li et al. (2012) have documented the exceptional electron transport capabilities of WS2 in dye-sensitized solar cells (DSSCs). Furthermore, WS2 can be deposited via solution processing or sputtering techniques at reduced temperatures, offering versatile fabrication pathways for solar cell applications.(Gourmelon et al., 1997; Hankare et al., 2009; Li et al., 2012; Lignier et al., 1997).

The option of a suitable HTL is essential to improving PSC performance and due to its special qualities and advantages, spiro-OMeTAD has generated a great deal of interest as a commonly utilized HTL material for PSCs. The original Spiro-OMeTAD material stands out as the first to exhibit outstanding hole mobility, facilitating the effective movement of positive charges (holes) away from the perovskite layer. This efficiency significantly contributes to a high short-circuit current density (Jsc) and, consequently, to the overall power conversion efficiency (PCE) (Kagan et al., 1999). The material's energy levels are tunable using dopants and additives, aligning closely with perovskite levels, and boosting charge extraction. In terms of processing advantages, the material offers easy solution processability through methods like spin-coating, making it simple, scalable, and cost-effective compared to vacuum deposition. Additionally, it forms dense and pinhole-free films upon deposition, ensuring efficient charge transport and minimizing leakage currents.(Leijtens et al., 2015) Despite its initial success, Spiro-OMeTAD faces roadblocks for widespread use in PSCs. Its high cost hinders affordability, while limited stability under illumination, heat, and moisture reduces longterm performance. The commonly used dopant, Li-TFSI, further degrades both layers, and certain perovskite compositions even dissolve it during processing, limiting its compatibility (Jeon et al., 2014). These barriers necessitate the development of improved HTMs with affordability, stability, and broader compatibility to truly unlock the potential of perovskite solar technology. In this simulation structure Cuprous oxide (Cu2O)

is used as a replacement of famous Spiro-OMeTAD material. due to its advantageous combination of properties. Firstly, Cu2O boasts high hole mobility, ensuring efficient transport of the positively charged carriers produced by light absorption in the absorber layer. Secondly, its bandgap and energy levels align well with the perovskite's valence band, minimizing energy barriers at the interface and facilitating smooth hole transfer, reducing energy losses. Moreover, Cu2O is an economical and easily accessible material, rendering it a viable option for largescale production compared to certain conventional Hole Transport Materials (HTMs). (Chatterjee & Pal, 2016) Furthermore, its simple processing techniques like chemical bath deposition or atomic layer deposition, compatible with low-temperature methods, make it scalable and cost-effective for integrating into PSC fabrication. Beyond these advantages, it's possible that Cu2O will improve PSC stability. by acting as a buffer layer, reducing detrimental interfacial recombination and degradation processes. While Cu2O shows significant promise, research efforts are ongoing to explore further improvements through doping with elements like selenium or tellurium, optimizing thickness and processing conditions, and addressing potential limitations like long-term stability in complete PSC devices. Overall, Cu2O is identified as an encouraging option for Hole Transport Materials (HTMs) within perovskite solar cells, presenting opportunities for the progress of efficient and cost-effective solar technology via continuous research and development initiatives.

2. Method

For researchers focused on solar cell development, identifying the optimal configuration and materials remains a significant challenge. This process can be streamlined using simulation tools. SCAPS(Burgelman et al., 2000, 2004) offers extensive capabilities, not limited to simulating up to seven distinct layers and calculating various parameters, including spectral response, energy bands, current-voltage (J-V) characteristics, and defect density, through the solution of three fundamental semiconductor equations. Its user-friendly interface facilitates operation under both illuminated and dark conditions. SCAPS's modeling methodologies delineate critical phenomena in photovoltaic systems, enabling a logical and methodical determination of the best operational conditions for each parameter.

This study examines the performance of relatively new perovskite like material namely tri-cesium di-antimonide bismuth (Cs₃Sb₂I₉) as the absorber layer along with tungsten disulfide (WS₂) material as an electron transport layer (ETL) and Cu₂O as hole transport layer (HTL) material. The preliminary layered architecture of the solar cell, comprising FTO/WS₂/Cs₃Sb₂I₉/Cu₂O/Metallic Back contact, is illustrated in Figure 2.

In the simulation, the illumination was provided by an AM 1.5G solar radiation spectrum, characterized by an intensity of 1000 W/m². In the perovskite layer, defects were modeled with a characteristic energy of 0.1 eV and were assumed to follow a neutral Gaussian distribution, positioned 0.6 electron volts above the valence band. Interfacial defects were treated as neutral isolated defects, exhibiting an energy distribution centered at 0.6 electron volts relative to the valence band. Critical material parameters were collated from previous experimental studies and are encapsulated in Table 1, serving to corroborate the legitimacy of the simulation outcomes.

In the current configuration created in the SCAPS simulator, the structure is exposed to light illumination from the FTO side,

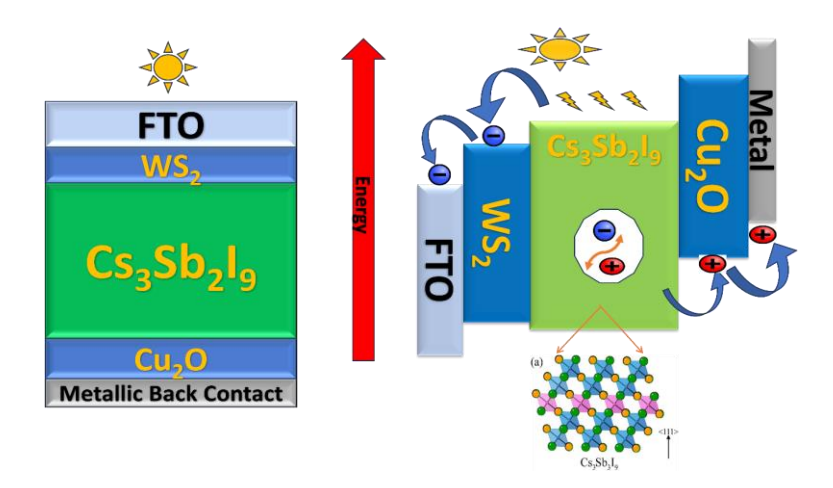


Fig 2. Schematic diagram of the solar cell structure

Table 1

Fundamental parameters employed in the SCAPS-1D simulation for each layer. **Parameters** FTO(Helander et WS2 (Abdelaziz et al., Cs₃Sb₂I₉(Thomas, Cu2O(Raoui et al., 2020; Sobayel et al., 2019; Wang et al., al., 2011) 2022a) 2019) 2015) Thickness (nm) 100 800 100 50 Bandgap (eV) 3.5 1.8 1.95 2.2 Electron affinity (eV) 4 3.95 4.5 3.4 Dielectric permittivity (relative) 9 13.6 4.19 7.5 2.2x10¹⁸ $2.0x10^{19}$ $1.0x10^{18}$ $1.0x10^{18}$ CB effective density of states (cm-3) $1.8x10^{19}$ 2.4x10¹⁹ 2.4x10¹⁹ $1.0x10^{19}$ VB effective density of states (cm⁻³) Electron mobility (cm²/Vs) 20 100 11.3 200 Hole mobility (cm²/Vs) 10 100 8600 5.58 1.0x10¹⁹ Shallow uniform donor density, ND (cm-3) $1.0x10^{18}$ 0 0 $1.0x10^{15}$ $1.0x10^{15}$ Shallow uniform acceptor density, N_A (cm⁻³) 0 0 1.0x1014 1.0x10¹⁴ 1.0x10¹⁴ $1.0x10^{14}$ Defect density N_t (cm⁻³)

utilizing the standard AM1.5 global spectrum (1000 W/m^2), with the default consideration of 100% light transmission. In this simulation, we explored the impact of light transmission into the structure by adjusting the transmission rate from 100% to 20%, and the corresponding J-V curve is depicted in Figure 3.

As depicted in Figure 3, it is evident that the transmission rate significantly impacts the short-circuit current rather than the voltage. As the transmission rate decreases, the photogenerated current also diminishes. This outcome serves

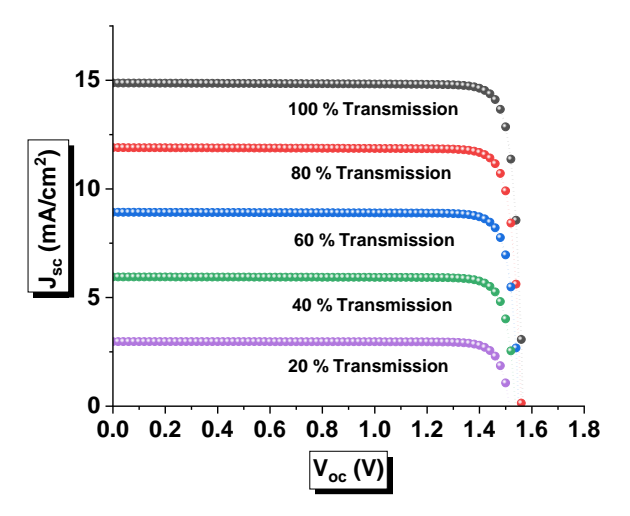


Fig 3 Variation of short circuit current density (J_{sc}) and open circuit voltage (V_{oc}) under different transmission rate

as validation for the credibility of the software employed to analyze the performance of the proposed solar cell structure. The series and shunt resistances for the cell are accounted for, and the frequency for the AC characteristics of the device is set at 1 MHz. The default operating temperature is established at 300 K. Table 1 shows the input parameters for each layer comprising the solar cell device. In this study, special emphasis has been placed on the defect density within both the perovskite absorber and charge transport layers, as well as on variations in electron affinity at the interfaces between the perovskite and the electron and hole transport layers, respectively.

The defect density, denoted as Nt, constitutes a critical parameter impacting solar cell performance. This density is characterized according to the Shockley–Read–Hall (SRH) model (Devi & Mehra, 2019) as written in equation. (1)

$$R = \frac{np - n_i^2}{\tau_p(n + N_{C^e}(E_g - E_t)/kT) + \tau_n(p + N_{V^e}(E_t)/kT)}$$
(1)

In this context, n and p symbolize the concentrations of electrons and holes, respectively, derived from solving the continuity and Poisson equations. The term ni^2 is disregarded under conditions where qV > 3kT, corresponding to a sufficient forward bias. The lifetimes of holes τ_p and electrons τ_n are intricately associated with the defect density, reflecting the substantial impact of defects on carrier recombination dynamics. Additionally, the carrier lifetime is a direct function of minority carrier diffusion length (L) by the following equation (2)(Baig *et al.*, 2018).

$$L_D = \sqrt{\frac{kT\mu_{(e,h)}}{q}\tau} \tag{2}$$

 $L_{\rm D}$ represents the diffusion length, with $\mu(e,h)$ indicating the mobilities of electrons and holes, respectively, and τ signifying the minority carrier lifetime. The lifetime of minority carriers is contingent upon the defect density and the capture cross-section area for both electrons and holes. The correlation between τ and the bulk defect density is delineated in Equation (3) (Baig et al., 2018) -

$$\tau = \frac{1}{N_t \delta v_{th}} \tag{3}$$

where δ represents the capture cross-section area for electrons and holes, v_{th} represents the thermal velocity of carriers, and N_t is traps density. In the context of shallow junction solar cells exhibiting prolonged minority carrier lifetimes within the perovskite material. The Internal Quantum Efficiency (IQE) may be influenced by the diffusion lengths of the minority carriers, as articulated in Equation (4).(Geist, 1979).

$$QE = 1 - \alpha t - \frac{B}{\alpha L^2} \tag{4}$$

In the equation, α represents the spectral absorption coefficient, t corresponds to the light penetration depth within the perovskite material, and B signifies the thickness of the perovskite layer.

3. Results and Discussion:

3.1. Effect of absorber layer thickness variation

The efficacy of solar cell devices is markedly affected by the absorber layer's thickness, necessitating comprehensive investigations into its dimensional variations. The operational performance of the device, correlated with the thickness of the $Cs_3Sb_2I_9$ perovskite layer, is depicted in Figure 4, where the thickness was varied between 0.5 μ m and 0.8 μ m.

It has been observed that an augmentation in absorber thickness results in a higher short-circuit current density, as

illustrated in Figure 4(b). This is attributed to the increased thickness allowing the absorption of more photons, particularly those of higher wavelengths. This, in turn, generates an excess number of carriers, preceding to a boost in the short-circuit current (J_{sc}) and subsequently improving efficiency, as indicated in Figure 4(a). However, when the thickness exceeds 0.8 µm, the Power Conversion Efficiency (PCE) value plateaus at around 20 % due to an increase in recombination and a decrease in the lifetime of the photo-generated charge carriers in the absorber layer (Hao *et al.*, 2021) . This phenomenon is also responsible for the lower values of open-circuit voltage (V_{oc}) and Fill Factor (FF) as the absorber layer thickness increases. (Chelvanathan *et al.*, 2010) So, the optimized thickness is taken to be 0.6 µm which trade off the open circuit voltage and short circuit current density values of the architecture.

An imperative factor linked with augmented thickness is the increment in series resistance, which consequentially diminishes the Fill Factor (FF). FF is pivotal in gauging solar cell efficacy, as it quantifies the capacity of the cell to transfer the generated power to a load and elucidates the internal power dissipation. In absorbers of increased thickness, the internal power loss is exacerbated, leading to a decline in FF. For optimizing Power Conversion Efficiency (PCE), it is essential that the carrier diffusion length surpasses the perovskite layer's thickness, thereby reducing recombination events. The absorber layer's thickness is intricately connected to both the minority carrier diffusion length (or carrier lifetime) and the defect density.

3.2. Effect of defect density variation of both absorber and charge transport layers:

An inverse relationship between defect density and carrier lifetime is established by Equation 3, as seen in the inset of Figure 5. Moreover, carrier lifetime is directly linked to the diffusion lengths of both electrons and holes. This implies that an increase in carrier lifetime results in a proportional increase in the mean free path, indicating that carriers travel a greater distance before experiencing recombination.

Figure 5 illustrates how the minority carrier diffusion length varies with the defect density of the $Cs_3Sb_2I_9$ perovskite layer. The graph clearly indicates that as the defect density of the absorber layer rises from 1E14 /cm³ to 1E16 /cm³, the

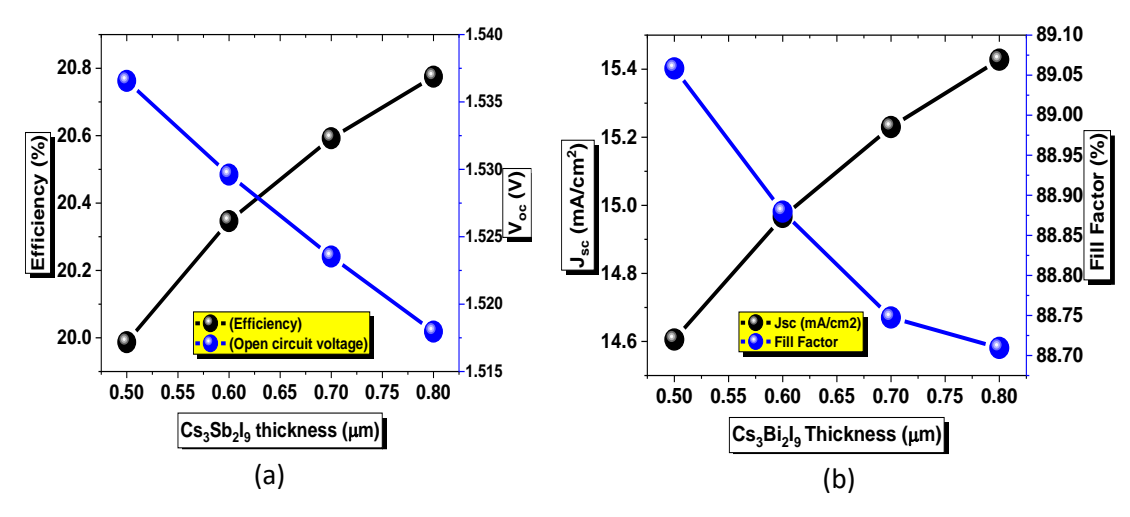


Fig 4 Variation of (a)Efficiency and open circuit voltage (V_{oc}) (b) Short circuit current density (J_{sc})and fill factor due to the thickness variation of $Cs_3Bi_2I_9$ absorber layer

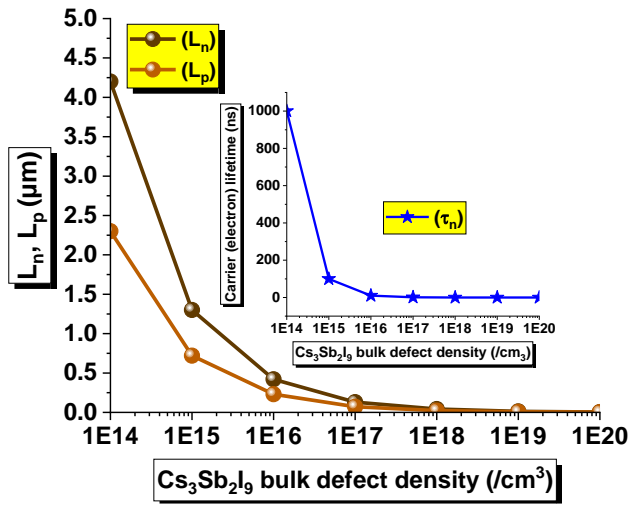


Fig. 5 Variation of minority carrier diffusion length of electrons and holes with the defect density of absorber layer (inset: electrons lifetime)

electron diffusion length significantly decreases from 4.3 um to 0.5 um, falling below the considered thickness of the perovskite layer in this simulation. As determined from Figure 4, the best possible thickness for the perovskite layer is approximately 0.6 um. To effectively collect photo-generated charge carriers, the minority carrier diffusion length must exceed the thickness of the absorber layer to prevent undesirable recombination. This recombination process leads to a reduction in carrier lifetime, signifying that a significant portion of the carriers will undergo recombination before reaching their respective contacts. As evident in the inset of Figure 5, the electron lifetime experiences a sharp decline from 1 μs to almost 0.1 μs with just a slight increase in defect density, going from 1E14 /cm³ to 1E15 /cm³.

Concerning hole diffusion length, the situation is more challenging than for electrons. In Figure 5, when the defect density reaches 1E15 /cm³, the hole diffusion length decreases below the width of the absorber layer. To address the influence of defect density, reducing the thickness of the perovskite layer is necessary. However, this approach is impractical due to the conflicting goals of achieving higher efficiency and maintaining ease of manufacturing.

In this research, a detailed discussion of the influence of defects has been done. Figure 6 shows the influence of defects

on main parameters of the device. In Figure 6(a), the efficiency graph demonstrates an exponential decrease, whereas the open-circuit voltage exhibits a nearly linear decline with increasing defect density. The power conversion efficiency decreases from 20.67% at a defect density of 1E14 /cm³ to below 5% at a defect density of 1E18 /cm³. The rise in defect density adversely affects the short circuit current density more than the open circuit voltage, as illustrated in Figures 6(a) and 6(b). Over the range of defect density varying from 1E14 /cm³ to 1e18 /cm³, the open circuit voltage decreases from 1.60 V to 1.10 V, while the short circuit current density drops from 15 mA/cm² to 9 mA/cm², consequently leading to a reduction in the fill factor.

Figure 7(a) exhibits the variation of short circuit current density (Jsc) in response to the increasing value of defect density. From Figure 7a, it is clearly stated that the defect imposes a detrimental effect on the short circuit current density reducing its value from 15 mA/cm² to 8 mA/cm² for the defect density range of 1E14 /cm³ to 1E20 /cm³. The open circuit voltage (Voc) is also hampered by the defect values. From equation 4, it has been seen that, the quantum efficiency is related to the minority carrier diffusion length and in turn the short-circuit current (Jsc)

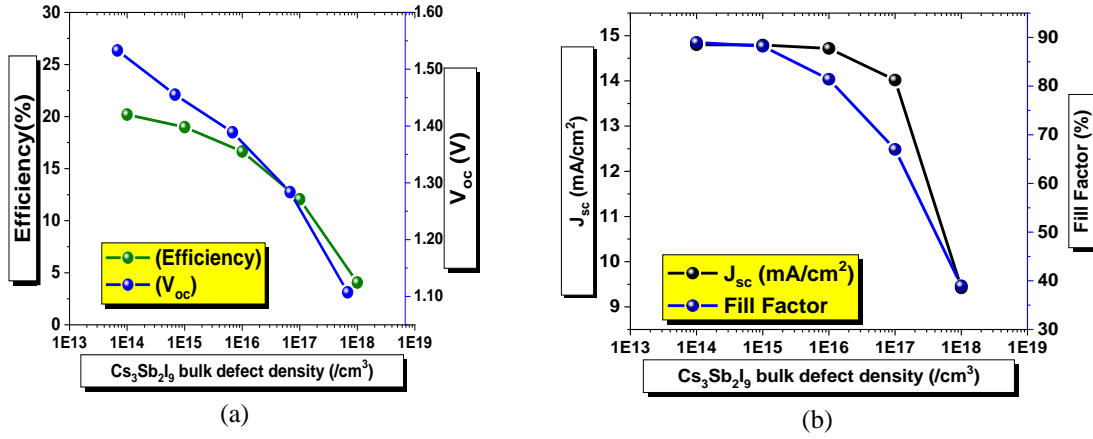


Fig 6 Variation of (a) Efficiency and open circuit voltage (V_{oc}) (b) Short circuit current density (J_{sc}) and fill factor due to the bulk defect density of $Cs_3Sb_2I_9$ absorber layer.

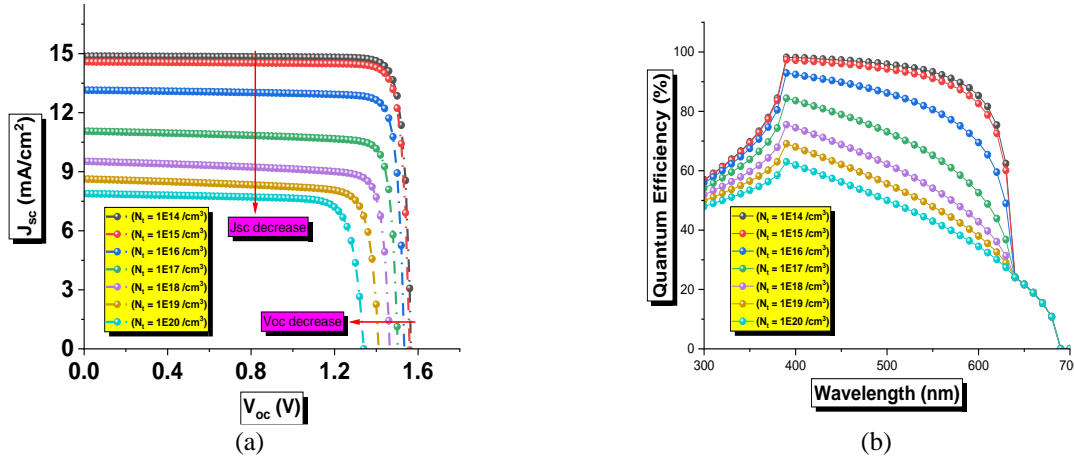


Fig 7 (a) Current-voltage characteristics curve of the device under varying defect density (b) Quantum Efficiency variation w.r.t the defect density changes.

Quantum efficiency (QE) is defined as the ratio of the number of generated electrons and holes to the number of electrons and holes collected at the electrodes. The proposed device exhibits excellent absorption, surpassing 90% for the visible spectrum of light within the wavelength range of 400 nm to 680 nm, as indicated by the topmost black line in Figure 7(b). However, the QE value experiences a significant reduction from 90% to 50% with increasing defect density values.

This decline can be elucidated by considering a hypothetical scenario where 100% of light transmission occurs through the device, and each incident photon generates an electron-hole pair to be collected at the respective contacts. However, at higher defect density values, the presence of numerous defects creates a substantial number of trap states, acting as recombination centers for the generated carriers as they move towards the electrode. Consequently, the number of collected carriers becomes much smaller than the number of generated carriers. In practical scenarios, not all photons may be absorbed to produce electron-hole pairs, owing to non-absorption and thermalization effects.

Perovskite devices are generally composed of multiple strata, encompassing perovskite (PVSK) light-absorbing layers

and electron/hole transport layers (ETLs/HTLs), configured in diverse architectures. (n-i-p or p-i-n). (Kim et al., 2023) In this simulation work, we have not only focused on the bulk defect of the absorber layer but also focus on the bulk defects of the charge transport layers. Figure 8 shows the behavior of the device in terms of main parameters w.r.t the variation of WS $_2$ material which is acting as the electron transport layer (ETL) of the structure.

Figure 8 demonstrates that all key parameters, including efficiency, open circuit voltage, short circuit current density, and fill factor, exhibit decreasing trends as the defect density increases with the defect density in the WS $_2$ layer ranges from 1E13 /cm 3 to 1E19 /cm 3 . The power conversion efficiency (PCE) of the structure decreases from 20.67% to 12% with the rise in defect values, and the fill factor follows a similar pattern. It is noteworthy that the bulk defects in the hole transport layer (HTL) material (Cu $_2$ O) have a minimal impact on the device's PCE. Within the same range of defect density values as the electron transport layer (ETL), the device's efficiency experiences only a marginal decrease of 0.002%. Consequently, it can be inferred that, for a highly efficient perovskite structure,

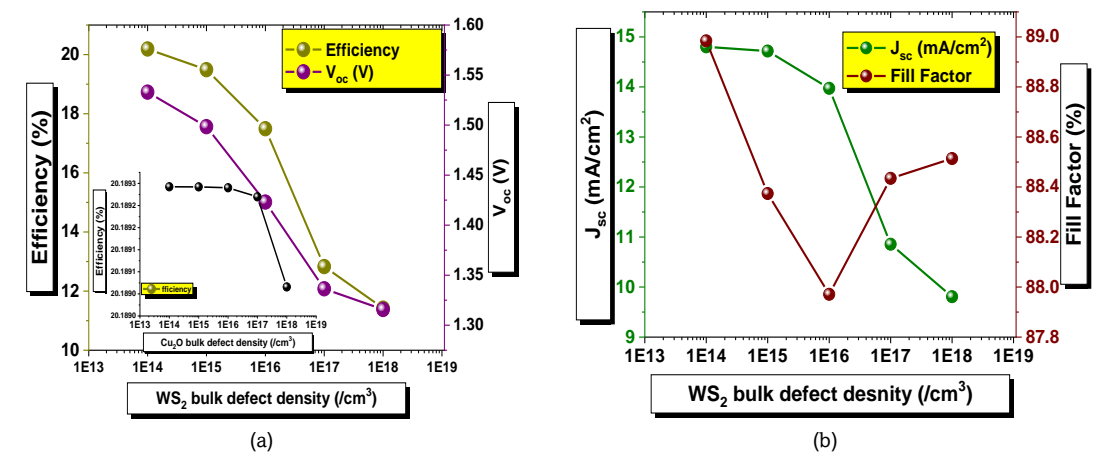


Fig-8 Variation of (a) Efficiency and open circuit voltage (V_{oc}) (b) short circuit current density (J_{sc}) and FF w.r.t the changes of bulk defect density of ETL (WS₂) material

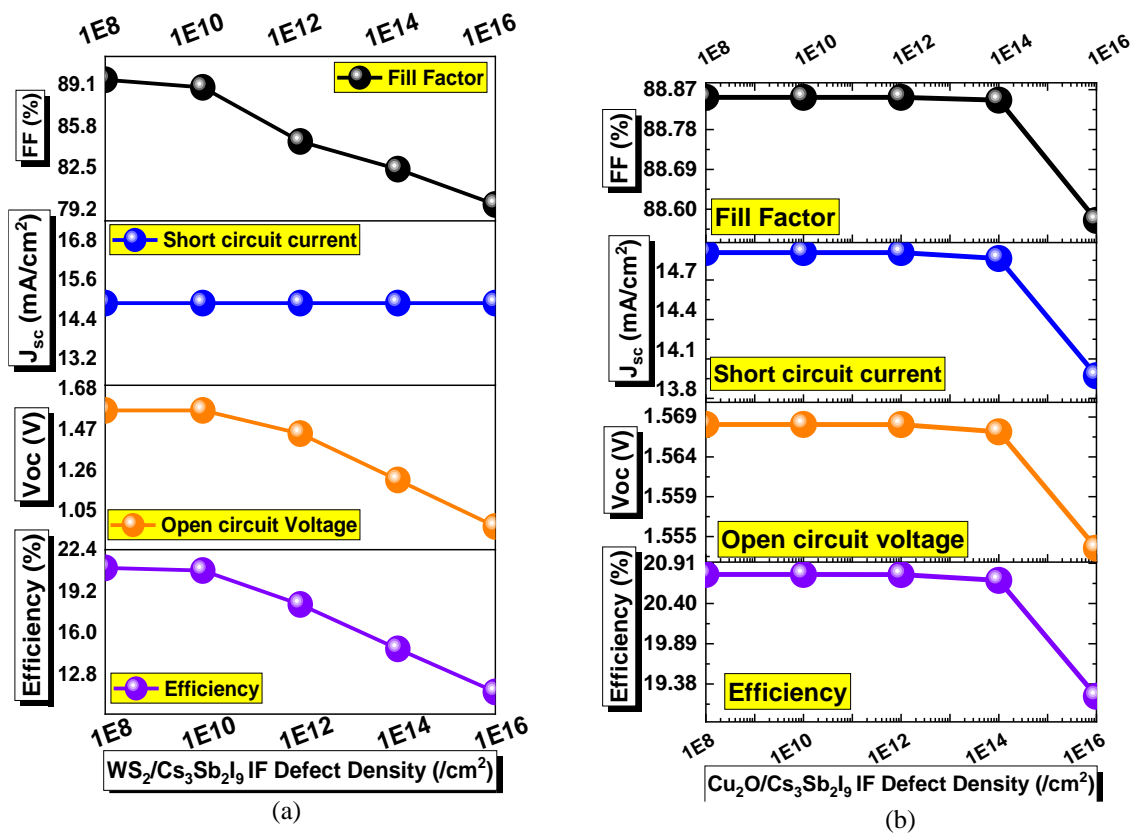


Fig 9. Variation of basic parameters w.r.t the interface defects (a) Defect density between WS₂/Cs₃Sb₂I₉ (b) Defect density of Cs₃Sb₂I₉/Cu₂O

ETL layers with minimal defects may be a more favorable choice.

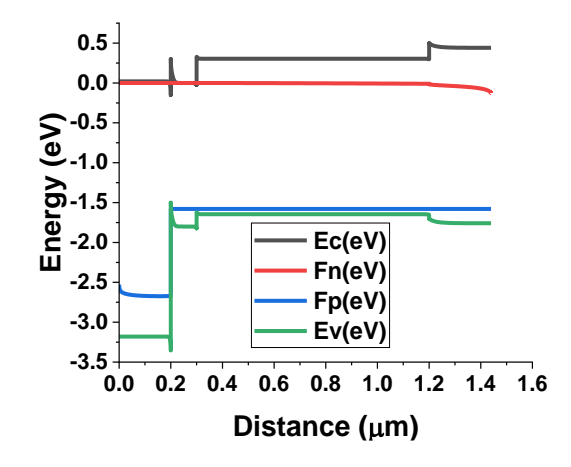
3.3. Influence of Interface (IF) defect density between the perovskite and the charge transport layers:

Interface between the perovskite and ETL and HTL layers play a significant rule on the performance of any solar cell structure. In this research, the effect of both $WS_2/Cs_3Sb_2I_9$ and $Cu_2O/Cs_3Sb_2I_9$ interface defects have been analyzed which is picturized in Figure 9.

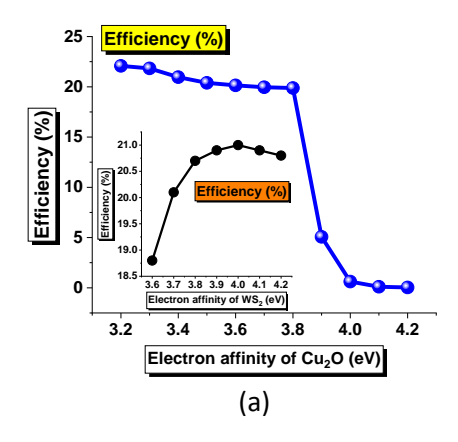
The presence of an intrinsic electric field in the interstitial region between the electron transport layer (ETL) or hole transport layer (HTL) and the perovskite interface facilitate the dissociation and transport of excitons, thereby expediting the migration of electrons and holes to their respective contacts. This investigation explores the impact of defect density concentration at the interface between the Cs3Bi2I9 absorber and the charge transport layers, elucidating its role in the photophysical processes pertinent to device performance. In Figure 9(a), the dependency of basic solar cell parameters on the defect density concentrations at the interfaces of the electron transport layer (ETL) and the absorber layer is illustrated. The data reveal a detrimental effect of interface defects on various performance metrics of solar cells, characterized by a consistent decline across all parameters as the interface defect density escalates from 1E10 /cm2 to 1E16/cm2 while defect density of 1E8 /cm2 has no effect on the performance of the cell. Specifically, the efficiency diminishes from 20.77% to 11.65 % in correlation with the increment in interface defect density. A similar pattern is observed for the interface defect density between the perovskite absorber layers and the hole transport layer (HTL). The solar cell parameters are shown in Figure 9(b) to be essentially unchanged up to a defect density of 1E14 /cm². However, it is important to note that the impact of defect density for this HTL/absorber interface is significantly less than the impact of ETL/absorber interface. It is evident from Figures 9(a) and 9(b) that the absorber/HTL interface experiences a substantially slower rate of efficiency decline than the ETL/absorber interface.

3.4. Effect of electron affinity variation

Energy band alignment critically influences the transport of photogenerated charge carriers, thereby dictating the photovoltaic (PV) efficacy of the engineered solar cell (SC).



 $\textbf{Fig 10} \ \textbf{Energy Band diagram of the proposed architecture}$



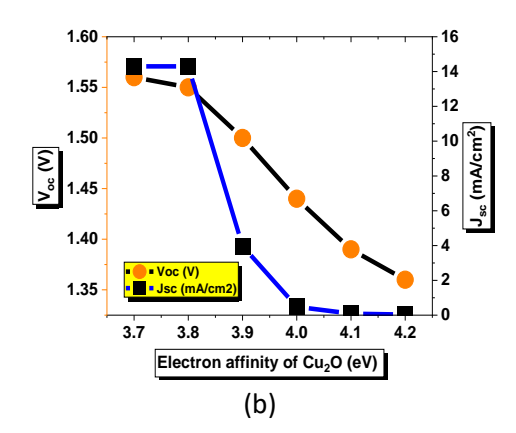


Fig-11 Variation of (a) Efficiency (b) Open circuit voltage and short circuit current density w.r.t the variation of electron affinity of Cu₂O layer. Fig-11(a) inset- Variation of efficiency w.r.t the electron affinity of WS₂ layer

(Hossain *et al.*, 2015) The configuration of energy bands as shown in Figure 10 is explicated by examining the electron affinity and the dynamics of band offsets at the junctures between the absorber and charge transport layers.

Electron affinity is precisely delineated as the energy differential between the conduction band minimum and the vacuum level within a semiconductor apparatus. In the context of heterostructure semiconductor devices, where the bandgap varies between the materials constituting the junction, the conventional flat-band diagram is not applicable. Consequently, the electron affinity undergoes alterations owing to shifts in the bandgap.

In Figure 11(a) and (b) the electron affinity values for both WS $_2$ (ETL) and Cu $_2$ O (HTL) are observed to fluctuate between 3.2 eV and 4.2 eV. It is evident that the power conversion efficiency (PCE) is significantly influenced by the electron affinity of the HTL layer in comparison to that of the ETL layer. The PCE experiences only a marginal change, ranging from 18.73% to 20.67%, as the electron affinity of the WS $_2$ layer varies from 3.6 eV to 4.2 eV, with the highest efficiency observed at an electron affinity value of 4.0 eV. The simulation indicates a convergence error for lower electron affinity values below 3.6 eV for the WS $_2$ layer.

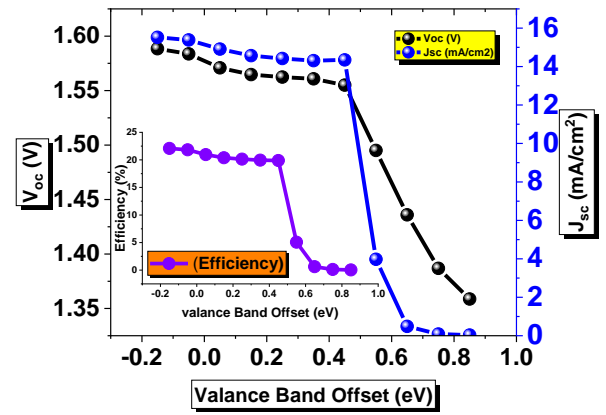


Fig 12. Variation of open circuit voltage ($V_{\rm oc}$) and short circuit current density ($J_{\rm sc}$) for the valance band offset values (inset: the power conversion efficiency)

In contrast to the efficiency changes attributed to WS2 variation, the alterations in PCE are relatively constant for electron affinity values ranging from 3.2 eV to 3.8 eV, pertains to the Cu2O layer. However, beyond 3.8 eV, the PCE values exhibit a sharp decline, plummeting from 23.34% to 5%. This decline is attributed to a reduction in both open circuit voltage and short circuit current density. The above effects can be discussed w.r.t the valance band offset (VBO) concept.

Figure 12 reveals that the valence band offset (VBO) for Cu₂O exhibits both negative and positive values. A negative VBO creates an energy cliff near the absorber/HTL interface, facilitating the movement of hole charge carriers. The corresponding power conversion efficiency (PCE) behavior is illustrated in the inset of Figure 12, where the PCE remains relatively constant at around 22% for band offset values ranging from -0.2 eV to +0.4 eV. However, beyond this range, both open circuit voltage and short circuit current density sharply decrease due to the formation of a spike-type band offset near the absorber/HTL interface. This spike hinders the movement of hole charge carriers, leading to a notable alteration in the efficiency of the designed solar cell, as depicted in the inset of Figure 12 (Benzetta *et al.*, 2020; Wang *et al.*, 2015).

3.5. Effect of Temperature (Activation Energy Analysis)

In this study, we conducted a thorough investigation into the thermal dependence of device performance by means of activation energy analysis, specifically observing the variation of open-circuit voltage ($V_{\rm oc}$) with respect to changes in temperature. This analysis was facilitated by the SCAPS-1D simulation environment, which inherently assumes a nominal operating temperature of 300 Kelvin. However, notable deviations in the simulation results were detected at temperatures below this standard, often manifesting as convergence errors within the simulation.

To accurately assess these variations, it became necessary to extend the V_{oc} -temperature relationship down to the theoretical limit of 0 K as temperature generated heat plays a big role not only in material levels but also in module levels.(AlSaleem et al., 2022; Alshammari et al., 2022; Najlaoui et al., 2023) This process involved extrapolating the observed data points to intersect the Y-axis (V_{oc}) at this absolute zero temperature, thereby estimating the absorber material's energy

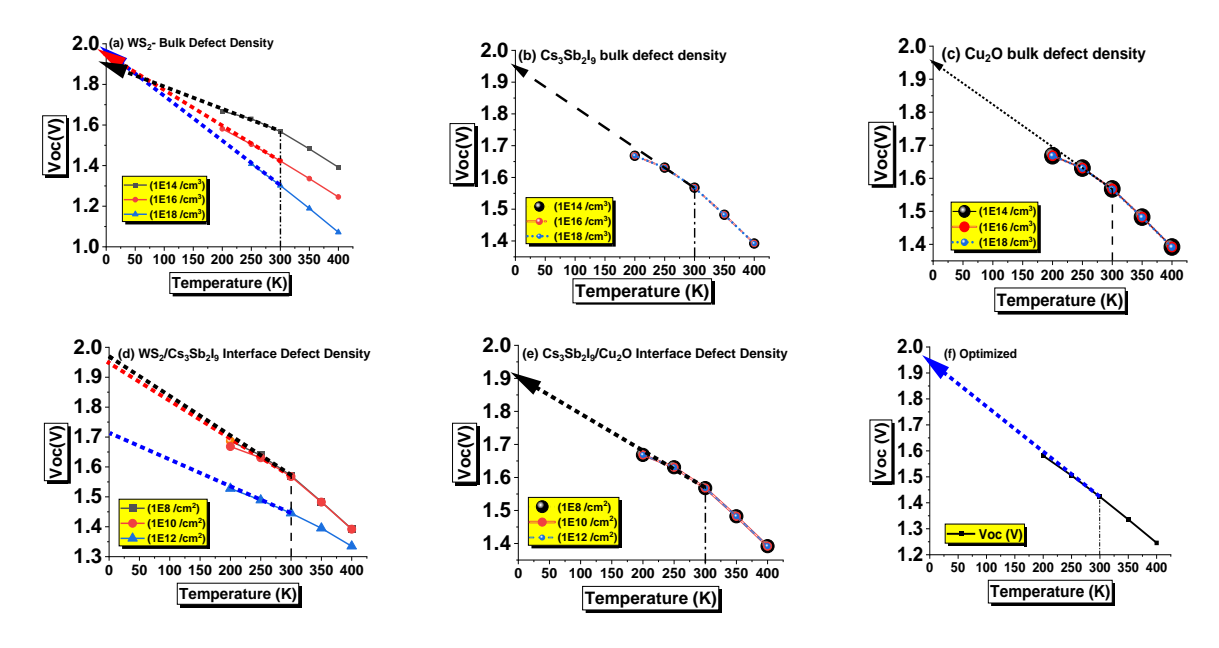


Fig 13 Open circuit voltage (V_{oc}) as a function of temperature (K) extrapolated to 0 K to find the activation energy (E_a) on various defects (a) Bulk defect of ETL material (WS₂), (b) Bulk defect of Absorber material (Cs₃Sb₂I₉) (c) bulk defect of HTL material (Cu₂O), (d) Interface Defects between WS₂/Cs₃Sb₂I₉ layers (e) Interface Defects between Cs₃Sb₂I₉/Cu₂O layers and (f) Optimized Results

gap. The rationale behind this approach lies in the assumption that, at 0K, all thermally activated recombination processes would cease, thus equating the open-circuit voltage with the material's bandgap. By drawing a tangent from the extrapolated line to its intersection point on the V_{oc} axis, we could infer the intrinsic energy gap of the absorber material. Should this tangent intersect at a voltage different from the anticipated bandgap, it would imply the persistence of recombination activities at 0K. Such a discrepancy would be indicative of inherent recombination dynamics within the device structure that are not solely thermally activated, thereby providing deeper insights into the material's behavior and the efficiency of the device under varied thermal conditions.

Figure 13 presents a detailed examination, where the relationship between temperature and open-circuit voltage (V_{oc}) has been scrutinized. This analysis encompasses an evaluation of the defects in both the individual absorber and charge transport layers, as well as the interfacial defects between the perovskite and charge transport layers.

Analysis of Figure 13 elucidates the critical role of defects within the electron transport layer (ETL) and its interface with the perovskite layers in modulating device performance through various recombination mechanisms, such as Schockley-Read-Hall (SRH), Radiative Recombination (RR), and Auger Recombination. The defect density in the bulk WS₂ layer was varied between 1E14 /cm³ and 1E18 /cm³revealing that elevated defect levels lead to a deviation of the open-circuit voltage (Voc) from the absorber material's designated bandgap. Specifically, Figure 13(a) indicates that when defect density is within 1E14 /cm³ to 1E16 /cm³, the Voc closely aligns with the 1.95 eV bandgap; however, an increase beyond 1E16 /cm³ widens the gap between the measured Voc and the theoretical bandgap, highlighting structural defects.

Similarly, the interface between WS_2 and $Cs_3Sb_2I_9$ significantly influences the recombination dynamics within the structure, as depicted in Figure 13(d). Interface defects at a density of 1E12 /cm2 result in a simulated V_{oc} of 1.7 eV, which is 0.25 eV below the bandgap, indicating substantial loss of

photogenerated carriers at the ETL-absorber interface, even at $0^{\circ}C$

Conversely, the interface between the hole transport layer (HTL) Cu_2O and the absorber exhibits a less pronounced effect on V_{oc} , with only a 0.04 eV shift observed as interface defect density increases from 1E8 /cm³ to 1E12 /cm³ (Figure 13(e)). Intriguingly, Figures 13(b) and (c) demonstrate that the bulk defects in both the absorber and HTL (Cu²O) maintain a consistent V_{oc} , aligning precisely with the absorber's bandgap, indicating the structural robustness against defects. The optimized structure depicted in Figure 13(f) substantiates the resilience of the perovskite material to defects, underscoring its potential for high-performance applications.

3.6. Effect of Series and Shunt Resistance

In empirical solar cell configurations, the existence of intrinsic resistive components, such as series and shunt resistances, precipitates a decline in operational efficacy, notwithstanding their exclusion from ideal structural considerations. Within simulation paradigms, the absorber stratum can be conceptualized as ideal, devoid of these resistive elements. However, for a comprehensive understanding of the influence exerted by series (R_s) and shunt (R_{sh}) resistances on the prototypical device function, these parameters are incorporated into the SCAPS framework. The values for R_s and R_{sh} are modulated within the ranges of 0-50 Ohm.cm² and 1E2 to 1E5 Ohm.cm², respectively. Subsequent evaluations of efficiency and fill factor are delineated in Figures 14(a) and 14(b).

Our results unequivocally indicate that an increase in series resistance (R_s) correlates with a marked reduction in the fill factor (FF), which diminishes from 93% to 66% for the device, as illustrated in Figure 14(a). Moreover, the efficiency of the device experiences a pronounced decline from 18.61% to 2% as the Rs value escalates to 50 Ohm·cm². In contrast, reductions in shunt resistance (R_{sh}) exert a more severe negative effect on both efficiency and fill factor than that observed for series

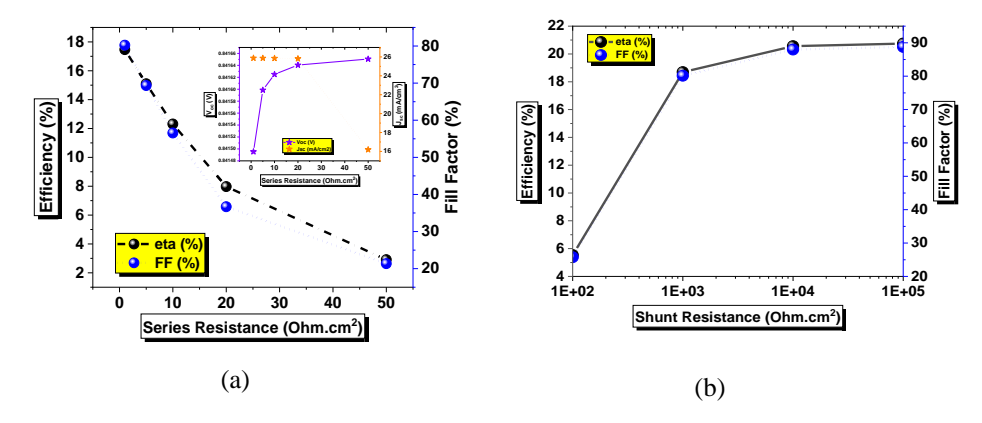


Fig 14 Effect of (a) series and (b) shunt resistance on the performance of the solar cell

resistance. As shown in Figure 14(b), at an $R_{\rm sh}$ value of 100 Ohm·cm², the efficiency and fill factor are reduced to 5% and 20%, respectively. Both metrics tend to stabilize when the $R_{\rm sh}$ value is increased beyond this point.

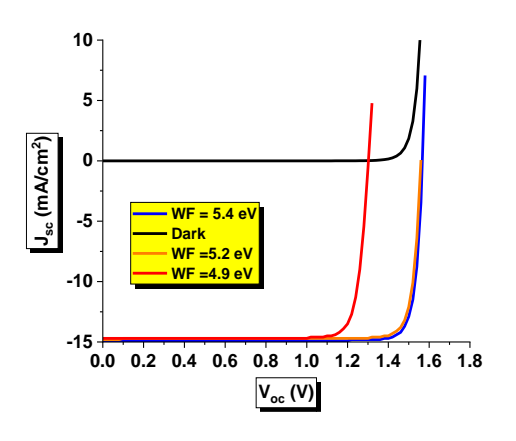
The origin of series resistance (R_s) is attributed to the electrical resistance associated not only with the terminal contacts but also with the electrical losses occurring within the electron and hole transport layers and the absorber material. On the other hand, shunt resistance (R_{sh}) represents various alternative pathways for charge recombination, significantly influenced by the device's structural design, particularly edge effects. Consequently, a low R_{sh} can lead to a reduction in photovoltage and adversely impact the harvested photocurrent. In contrast, R_s predominantly affects the fill factor (FF) and the short-circuit current density (Jsc). It is universally recognized that minimizing R_s and maximizing R_{sh} are essential for the realization of highly efficient photovoltaic devices.

3.7. Effect of metal work function at the back contact and back surface filed (BSF) layer:

Selecting an appropriate back contact metal is critical for the performance of solar cells. In SCAPS 1d simulations, a flat band model is employed for the back contact metal electrode, presuming ohmic contact with the hole transport layer (HTL) semiconductor material, although this assumption often does not hold in practice. Due to material disparities at the interface between the semiconductor and metals, a Schottky-type contact rather than an ohmic contact is typically formed,

hindering the transport of photogenerated holes from the absorber to the back contact via the HTL. The formation of Schottky contacts, associated with lower metal work function values, can impair solar cell performance. To mitigate this issue, metals with higher work function values are preferred to establish better ohmic or near-ohmic contacts at the metal/semiconductor interface. Empirical data in Figure 15 (b) indicate that a work function value exceeding 5.1 eV yields a peak power conversion efficiency (PCE) of approximately 21.6%, although the benefit plateaus beyond this threshold, indicating the establishment of an effective contact between Cu₂O and the metal. Precious metals like Au and Pt, with higher work functions, are theoretically ideal but economically impractical for cost-effective solar cell designs. Conversely, reducing the work function value below a certain threshold can induce a crossover effect, where the illuminated current-voltage (JV) curve intersects the dark IV curve, leading to a significant reduction in open-circuit voltage. For instance, a work function of 4.9 eV (represented in red on the graph 15(a)) demonstrates a lower voltage than the dark IV characteristics, with simulation errors occurring below this work function value.

Enhancing solar cell performance can also be achieved by integrating a highly doped thin back surface field (BSF) layer, which serves as a conduit between the hole transport layer (HTL) and the metal contact. The rationale for this approach lies in the mobility discrepancy between the HTL material, which has lower hole mobility, and the metal, which is highly conductive but requires carriers that the semiconductor cannot



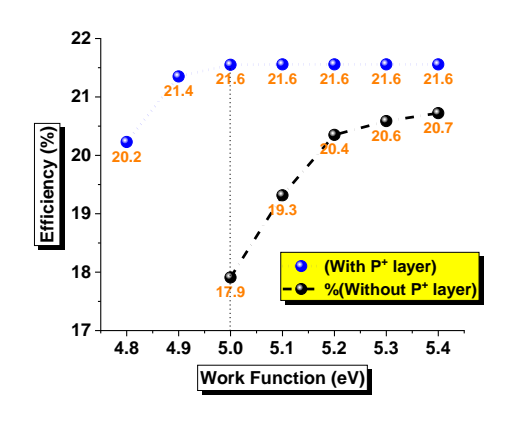


Fig 15 (a). Cross-over effect (b) Metal work function vs Efficiency with and without p+ thin layer

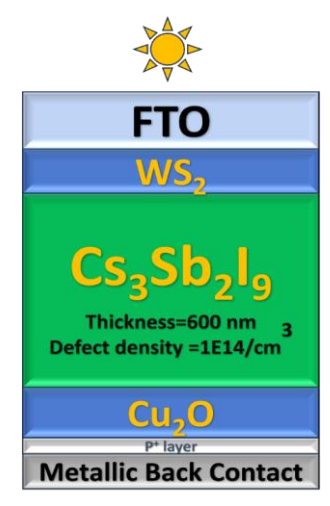


Fig 16 Optimized structure of the proposed solar cell

sufficiently provide, leading to an interface disparity. Introducing a heavily doped p-type (p+) layer between the HTL and the metal contact forms a p-p+ junction, facilitating nearohmic behavior and enhancing hole transport. In our study, we employed a p+ thin layer as the BSF to address these challenges, resulting in notable improvements in both the efficiency and the flexibility of reducing the metal work function, as demonstrated in Figure 15(b). Without the p+ layer, the metal work function could not be reduced below 5 eV without compromising performance. However, with the p+ layer incorporated as the BSF, we not only achieved an elevated efficiency of approximately 21.6% at a work function of 5.1 eV but also maintained efficiencies above 20% with metal work function values down to 4.8 eV. This underscores the effectiveness of the BSF layer, which additionally serves as a surface passivation layer. The optimized structure is depicted in Figure 16.

9. Conclusion

This scholarly article delves into the efficacy of Cesium Antimonide Iodide (Cs3Sb2I9) as a light-harvesting component in tandem with the renowned transition metal sulfide, WS2, for electron transport and Cu2O for hole transport, to construct an all-inorganic perovskite-based solar cell. Employing the SCAPS 1D simulation tool, the research meticulously evaluates critical design parameters, emphasizing the efficiency of the photovoltaic architecture under study. The scope of analysis spans the variations in thickness, doping intensities, and defect densities, including both bulk and interfacial defects, within the essential layers of the solar cell, namely the Electron Transport Layer (ETL), the absorber layer, and the Hole Transport Layer (HTL). The study extends to assess additional structural attributes such as diffusion length, activation energy, impacts of series and shunt resistances, and the metal work function. Notably, electron and hole diffusion lengths were determined to be 4.3 µm and 2.3 µm, respectively, at an absorber defect density of 1E14/cm3. The electron affinity of the WS2 layer has been identified as a significant determinant in the cell's performance, with the structure maintaining near-constant efficiency for valence band offset (VBO) values ranging from -0.2 eV to +0.4 eV. Optimal performance necessitates a series resistance below 10 Ohm.cm² and a shunt resistance exceeding 1000 Ohm.cm². Activation energy analysis further reveals that recombination processes at the ETL layer and its interface with the absorber have a profound impact, surpassing that at the HTL and its interface. Incorporating a heavily doped p-type back

surface field layer enhances the overall efficiency to 21.61%, enabling the utilization of metal back contacts with lower work functions, such as 5 eV or below. This strategy circumvents the economic challenges of employing materials with higher work functions, thereby advocating for a cost-effective solar structure that does not compromise on performance.

Acknowledgments

Researchers would like to thank the Deanship of Scientific Research, Qassim University for funding the publication of this project.

Data availability statement

All data that support the findings of this study are included within the article (and any supplementary files).

Conflicts of interest

The authors declare no conflict of interest.

References

- Abdelaziz, S., Zekry, A., Shaker, A., & Abouelatta, M. (2020). Investigating the performance of formamidinium tin-based perovskite solar cell by SCAPS device simulation. *Optical Materials*, 101, 109738. https://doi.org/10.1016/J.OPTMAT.2020.109738
- AlSaleem, S. S., Al-Qadami, E., Korany, H. Z., Shafiquzzaman, M., Haider, H., Ahsan, A., Alresheedi, M., AlGhafis, A., & AlHarbi, A. (2022). Computational Fluid Dynamic Applications for Solar Stills Efficiency Assessment: A Review. *Sustainability*, Vol. 14, Page 10700, 14(17), 10700. https://doi.org/10.3390/SU141710700
- Alshammari, F., Pesyridis, A., Alshammari, A. S., Alghafis, A., Alatawi, I., & Alzamil, A. (2022). Potential of capturing transportation wasted heat for better fuel economy and electricity generation: Comprehensive testing. *Energy Conversion and Management*, 267, 115939. https://doi.org/10.1016/J.ENCONMAN.2022.115939
- Baig, F., Khattak, Y. H., Marí, B., Beg, S., Ahmed, A., & Khan, K. (2018). Efficiency Enhancement of CH3NH3SnI3 Solar Cells by Device Modeling. *Journal of Electronic Materials*, 47(9), 5275–5282. https://doi.org/10.1007/S11664-018-6406-3/METRICS
- Benzetta, A. E. H., Abderrezek, M., & Djeghlal, M. E. (2020). A comparative study on generation and recombination process of kesterite CZTS based thin film solar cells for different designs. *Optik*, 219. https://doi.org/10.1016/J.IJLEO.2020.165300
- Boopathi, K. M., Karuppuswamy, P., Singh, A., Hanmandlu, C., Lin, L., Abbas, S. A., Chang, C. C., Wang, P. C., Li, G., & Chu, C. W. (2017). Solution-processable antimony-based light-absorbing materials beyond lead halide perovskites. *Journal of Materials Chemistry*, 5(39), 20843–20850. https://doi.org/10.1039/C7TA06679A
- Burgelman, M., Nollet, P., & Degrave, S. (2000). Modelling polycrystalline semiconductor solar cells. *Thin Solid Films*, 361, 527–532. https://doi.org/10.1016/S0040-6090(99)00825-1
- Burgelman, M., Verschraegen, J., Degrave, S., & Nollet, P. (2004).

 Modeling thin-film PV devices. *Progress in Photovoltaics: Research and Applications*, 12(2–3), 143–153.

 https://doi.org/10.1002/PIP.524
- Chatterjee, S., & Pal, A. J. (2016). Introducing Cu2O Thin Films as a Hole-Transport Layer in Efficient Planar Perovskite Solar Cell Structures. *Journal of Physical Chemistry C*, 120(3), 1428–1437. https://doi.org/10.1021/ACS.JPCC.5B11540
- Chelvanathan, P., Hossain, M. I., & Amin, N. (2010). Performance analysis of copper–indium–gallium–diselenide (CIGS) solar cells with various buffer layers by SCAPS. *Current Applied Physics*, 10(3), S387–S391. https://doi.org/10.1016/J.CAP.2010.02.018
- Correa-Baena, J. P., Luo, Y., Brenner, T. M., Snaider, J., Sun, S., Li, X., Jensen, M. A., Hartono, N. T. P., Nienhaus, L., Wieghold, S., Poindexter, J. R., Wang, S., Meng, Y. S., Wang, T., Lai, B., Holt, M. V., Cai, Z., Bawendi, M. G., Huang, L., ... Fenning, D. P.

- (2019). Homogenized halides and alkali cation segregation in alloyed organic-inorganic perovskites. *Science* (New York, N.Y.), 363(6427), 627–631. https://doi.org/10.1126/SCIENCE.AAH5065
- Dasgupta, U., Chatterjee, S., & Pal, A. J. (2017). Thin-film formation of 2D MoS2 and its application as a hole-transport layer in planar perovskite solar cells. *Solar Energy Materials and Solar Cells*, 172, 353–360. https://doi.org/10.1016/J.SOLMAT.2017.08.012
- Devi, C., & Mehra, R. (2019). Device simulation of lead-free MASnI3 solar cell with CuSbS2 (copper antimony sulfide). *Journal of Materials Science*, 54(7), 5615–5624. https://doi.org/10.1007/S10853-018-03265-Y/METRICS
- Eperon, G. E., Burlakov, V. M., Docampo, P., Goriely, A., & Snaith, H. J. (2014). Morphological Control for High Performance, Solution-Processed Planar Heterojunction Perovskite Solar Cells. Advanced Functional Materials, 24(1), 151–157. https://doi.org/10.1002/ADFM.201302090
- Geist, J. (1979). Quantum efficiency of the p-n junction in silicon as an absolute radiometric standard. *Applied Optics*, 18(6), 760. https://doi.org/10.1364/AO.18.000760
- Geng, W., Tong, C. J., Liu, J., Zhu, W., Lau, W. M., & Liu, L. M. (2016). Structures and Electronic Properties of Different CH3NH3PbI3/TiO2 Interface: A First-Principles Study. Scientific Reports 2016 6:1, 6(1), 1–8. https://doi.org/10.1038/srep20131
- Gourmelon, E., Lignier, O., Hadouda, H., Couturier, G., Bernède, J. C., Tedd, J., Pouzet, J., & Salardenne, J. (1997). MS2 (M = W, Mo) photosensitive thin films for solar cells. *Solar Energy Materials and Solar Cells*, 46(2), 115–121. https://doi.org/10.1016/S0927-0248(96)00096-7
- Hankare, P. P., Manikshete, A. H., Sathe, D. J., Chate, P. A., Patil, A. A., & Garadkar, K. M. (2009). WS2 thin films: Opto-electronic characterization. *Journal of Alloys and Compounds*, 479(1–2), 657–660. https://doi.org/10.1016/J.JALLCOM.2009.01.024
- Hao, L., Li, T., Ma, X., Wu, J., Qiao, L., Wu, X., Hou, G., Pei, H., Wang, X., & Zhang, X. (2021). A tin-based perovskite solar cell with an inverted hole-free transport layer to achieve high energy conversion efficiency by SCAPS device simulation. *Optical and Quantum Electronics*, 53(9), 1–17. https://doi.org/10.1007/S11082-021-03175-5/METRICS
- Hayat, M. B., Ali, D., Monyake, K. C., Alagha, L., & Ahmed, N. (2019). Solar energy—A look into power generation, challenges, and a solar-powered future. *International Journal of Energy Research*, 43(3), 1049–1067. https://doi.org/10.1002/ER.4252
- Helander, M. G., Greiner, M. T., Wang, Z. B., Tang, W. M., & Lu, Z. H. (2011). Work function of fluorine doped tin oxide. *Journal of Vacuum Science & Technology A: Vacuum, Surfaces, and Films*, 29(1). https://doi.org/10.1116/1.3525641
- Hossain, M. I., Alharbi, F. H., & Tabet, N. (2015). Copper oxide as inorganic hole transport material for lead halide perovskite based solar cells. *Solar Energy*, 120, 370–380. https://doi.org/10.1016/J.SOLENER.2015.07.040
- Huang, P., Wang, Z., Liu, Y., Zhang, K., Yuan, L., Zhou, Y., Song, B., & Li, Y. (2017). Water-Soluble 2D Transition Metal Dichalcogenides as the Hole-Transport Layer for Highly Efficient and Stable p-i-n Perovskite Solar Cells. *ACS Applied Materials and Interfaces*, 9(30), 25323–25331. https://doi.org/10.1021/ACSAMI.7B06403/SUPPL_FILE/AM 7B06403_SI_001.PDF
- Islam, M. S., Sobayel, K., Al-Kahtani, A., Islam, M. A., Muhammad, G., Amin, N., Shahiduzzaman, M., & Akhtaruzzaman, M. (2021). Defect study and modelling of SnX3-based perovskite solar cells with SCAPS-1D. *Nanomaterials*, 11(5). https://doi.org/10.3390/NANO11051218
- Jeon, N. J., Noh, J. H., Kim, Y. C., Yang, W. S., Ryu, S., & Seok, S. II. (2014). Solvent engineering for high-performance inorganicorganic hybrid perovskite solar cells. *Nature Materials* 2014 13:9, 13(9), 897–903. https://doi.org/10.1038/nmat4014
- Jin, Z., Zhang, Z., Xiu, J., Song, H., Gatti, T., & He, Z. (2020). A critical review on bismuth and antimony halide based perovskites and their derivatives for photovoltaic applications: recent advances and challenges. *Journal of Materials Chemistry A*, 8(32), 16166– 16188. https://doi.org/10.1039/D0TA05433J
- Kagan, C. R., Mitzi, D. B., & Dimitrakopoulos, C. D. (1999). Organic-Inorganic Hybrid Materials as Semiconducting Channels in Thin-

- Film Field-Effect Transistors. *Science*, 286(5441), 945–947. https://doi.org/10.1126/SCIENCE.286.5441.945
- Kim, S., Jeong, Y., Han, D. W., & Mo, C. Bin. (2023). Machine Learning-Assisted Defect Analysis and Optimization for P-I-N-Structured Perovskite Solar Cells. *Journal of Electronic Materials*, 52(9), 5861–5871. https://doi.org/10.1007/S11664-023-10533-4/METRICS
- Leccisi, E., & Fthenakis, V. (2020). Life-cycle environmental impacts of single-junction and tandem perovskite PVs: A critical review and future perspectives. *Progress in Energy*, 2(3). https://doi.org/10.1088/2516-1083/AB7E84
- Leijtens, T., Eperon, G. E., Noel, N. K., Habisreutinger, S. N., Petrozza, A., & Snaith, H. J. (2015). Stability of Metal Halide Perovskite Solar Cells. *Advanced Energy Materials*, 5(20), 1500963. https://doi.org/10.1002/AENM.201500963
- Leijtens, T., Eperon, G. E., Pathak, S., Abate, A., Lee, M. M., & Snaith, H. J. (2013). Overcoming ultraviolet light instability of sensitized TiO2 with meso-superstructured organometal tri-halide perovskite solar cells. *Nature Communications* 2013 4:1, 4(1), 1–8. https://doi.org/10.1038/ncomms3885
- Li, S., Chen, Z., & Zhang, W. (2012). Dye-sensitized solar cells based on WS 2 counter electrodes. *Materials Letters*, 72, 22–24. https://doi.org/10.1016/J.MATLET.2011.12.052
- Lignier, O., Couturier, G., Tedd, J., Gonbeau, D., & Salardenne, J. (1997).

 Photoactivity enhancement of WS2 sputtered thin films by use of nickel. *Thin Solid Films*, 299(1–2), 45–52. https://doi.org/10.1016/S0040-6090(96)09319-4
- Liu, C., Wang, K., Yi, C., Shi, X., Du, P., Smith, A. W., Karim, A., & Gong, X. (2015). Ultrasensitive solution-processed perovskite hybrid photodetectors. *Journal of Materials Chemistry C*, 3(26), 6600–6606. https://doi.org/10.1039/C5TC00673B
- Liu, D., & Kelly, T. L. (2013). Perovskite solar cells with a planar heterojunction structure prepared using room-temperature solution processing techniques. *Nature Photonics* 2013 8:2, 8(2), 133–138. https://doi.org/10.1038/nphoton.2013.342
- Liu, J., Zhuang, D., Luan, H., Cao, M., Xie, M., & Li, X. (2013).

 Preparation of Cu(In,Ga)Se2 thin film by sputtering from Cu(In,Ga)Se2 quaternary target. *Progress in Natural Science: Materials International*, 23(2), 133–138. https://doi.org/10.1016/J.PNSC.2013.02.006
- Liu, M., Johnston, M. B., & Snaith, H. J. (2013). Efficient planar heterojunction perovskite solar cells by vapour deposition. *Nature* 2013 501:7467, 501(7467), 395–398. https://doi.org/10.1038/nature12509
- Najlaoui, B., Alghafis, A., & Nejlaoui, M. (2023). Robust design of a low cost flat plate collector under uncertain design parameters. *Energy Reports*, 10, 2950–2961. https://doi.org/10.1016/J.EGYR.2023.09.039
- Raoui, Y., Ez-Zahraouy, H., Tahiri, N., El Bounagui, O., Ahmad, S., & Kazim, S. (2019). Performance analysis of MAPbI3 based perovskite solar cells employing diverse charge selective contacts: Simulation study. *Solar Energy*, 193, 948–955. https://doi.org/10.1016/J.SOLENER.2019.10.009
- Schileo, G., & Grancini, G. (2021). Lead or no lead? Availability, toxicity, sustainability and environmental impact of lead-free perovskite solar cells. *Journal of Materials Chemistry C*, 9(1), 67–76. https://doi.org/10.1039/D0TC04552G
- Sobayel, K., Akhtaruzzaman, M., Rahman, K. S., Ferdaous, M. T., Al-Mutairi, Z. A., Alharbi, H. F., Alharthi, N. H., Karim, M. R., Hasmady, S., & Amin, N. (2019). A comprehensive defect study of tungsten disulfide (WS2) as electron transport layer in perovskite solar cells by numerical simulation. *Results in Physics*, 12, 1097–1103. https://doi.org/10.1016/J.RINP.2018.12.049
- Sobayel, K., Rahman, K. S., Karim, M., Aijaz, M., Dar, M., Shar, M. A., Misran, H., & Amin, N. (2018). Numerical modeling on prospective buffer layers for tungsten di-sulfide (WS2) solar cells by scaps-1D. *Chalcogenide Letters*.
- Thomas, A. S. (2022a). A Review on Antimony-based Perovskite Solar Cells. Equilibrium Journal of Chemical Engineering, 6(2), 75. https://doi.org/10.20961/EQUILIBRIUM.V6I2.64322
- Thomas, A. S. (2022b). High-Efficiency Dye-Sensitized Solar Cells: A Comprehensive Review. *Computational And Experimental Research In Materials And Renewable Energy*, 5(1), 1. https://doi.org/10.19184/CERIMRE.V5I1.31475

Wang, Y., Xia, Z., Liu, Y., & Zhou, H. (2015). Simulation of perovskite solar cells with inorganic hole transporting materials. 2015 IEEE 42nd Photovoltaic Specialist Conference, PVSC 2015. https://doi.org/10.1109/PVSC.2015.7355717

Yang, G., Tao, H., Qin, P., Ke, W., & Fang, G. (2016). Recent progress in electron transport layers for efficient perovskite solar cells.

Journal of Materials Chemistry, 4(11), 3970–3990. https://doi.org/10.1039/C5TA09011C

Zhao, Y., & Zhu, K. (2016). Organic–inorganic hybrid lead halide perovskites for optoelectronic and electronic applications. *Chemical Society Reviews*, 45(3), 655–689. https://doi.org/10.1039/C4CS00458B



© 2024. The Author(s). This article is an open access article distributed under the terms and conditions of the Creative Commons Attribution-ShareAlike 4.0 (CC BY-SA) International License (http://creativecommons.org/licenses/by-sa/4.0/)